Improved B-spline image registration between exhale and inhale lung CT images based on intensity and gradient orientation information

Woo Hyun Nam[a], Jihun Oh[a], Jonghyon Yi[b], Yongsup Park[a], Hansu Cho[a], Sukjin Kim[a]
[a]Convergence Media Team, DMC R&D Center, Samsung Electronics Co. Ltd.,
Seoul R&D Campus, 34, Seongchon-gil, Seocho-gu, Seoul, 06765, South Korea
[b]Advanced R&D Team, HME Business, Samsung Electronics Co. Ltd.,
129, Samsung-ro, Yeongtong-gu, Suwon-si, Gyeonggi-do, 443742, South Korea

ABSTRACT

Registration of lung CT images acquired at different respiratory phases is clinically relevant in many applications, such as follow-up analysis, lung function analysis based on mechanical elasticity, or pulmonary airflow analysis, etc. In order to find accurate and reliable transformation for registration, a proper choice of dissimilarity measure is important. Even though various intensity-based measures have been introduced for precise registration, the registration performance may be limited since they mainly take intensity values into account without effectively considering useful spatial information. In this paper, we attempt to improve the non-rigid registration accuracy between exhale and inhale CT images of the lung, by proposing a new dissimilarity measure based on gradient orientation representing the spatial information in addition to vessel-weighted intensity and normalized intensity information. Since it is necessary to develop non-rigid registration that can account for large lung deformations, the B-spline free-form deformation (FFD) is adopted as the transformation model. The experimental tests for six clinical datasets show that the proposed method provides more accurate registration results than competitive registration methods.

Keywords: B-spline image registration, lung, CT, dissimilarity measure, gradient orientation information

1. INTRODUCTION

Lung registration between CT images obtained at different respiratory phases has become essential for various pulmonary image based applications, such as treatment planning [1]-[3], quantitative assessments [4]-[5], and motion analyses [6]-[7]. For more reliable utilization of the applications, accurate registration is required. To achieve this, many novel registration algorithms have been presented, which commonly used intensity information in their similarity (or dissimilarity) measures, such as intensity difference [8]-[9], mutual information or normalized cross correlation [10]-[11], and preserving tissue volume or lung mass [12]-[13]. Because they do not utilize the useful spatial anatomical information, the registration performance may be limited in important anatomical structures, such as small vessels and airways.

As a trial to improve the accuracy, the similarity measure which adds the vesselness information to the intensity information was introduced in [14], and it showed significantly improved accuracy compared to the methods using intensity information only. Since vesselness information can encode the spatial information mostly on apparent tubular structures, however, the similarity measure needs to be further improved to enhance the registration accuracy even on the other structures such as fissures and lung surfaces, and ambiguous tubular structures due to low intensity contrast.

In this paper, we introduce a new dissimilarity measure that uses gradient orientation information in addition to the vessel-weighted intensity and normalized intensity information. Since the proposed measure effectively manipulates both intensity and spatial correlation, we can further enhance the non-rigid registration accuracy.

The remainder of this paper is organized as follows. Section 2 describes the registration framework based on the proposed dissimilarity measure. In section 3, experimental results with quantitative and qualitative evaluations are described for six clinical datasets. Finally, conclusion is given in section 4.

Medical Imaging 2016: Image Processing, edited by Martin A. Styner,
Elsa D. Angelini, Proc. of SPIE Vol. 9784, 978440 · © 2016 SPIE
CCC code: 1605-7422/16/$18 · doi: 10.1117/12.2217390

2. THE PROPOSED METHOD

In this paper, we focus on the pulmonary image registration. Hence, we first exclude the regions other than the lung in each image through the segmentation based on an intensity thresholding method with a morphological closing. To include the nodules at the lung boundaries, a convex-hulling-based refinement is applied [15]. Using the segmentation results, binary lung masks are generated by morphologically dilating the segmented lung with a margin of 2 voxels. The masks for exhale and inhale images are denoted as M_{exhale} and M_{inhale} , respectively. For the masked region, we perform the conventional sum of squired-intensity-difference (SSID)-based affine registration with down-hill simplex optimization [16] to compensate for the global deformation between the two images. Using the obtained affine parameters, $\boldsymbol{\Theta}$, as an initial global transformation, we then apply the proposed non-rigid registration algorithm (see figure 1(a).). The proposed algorithm is described in detail in the following.

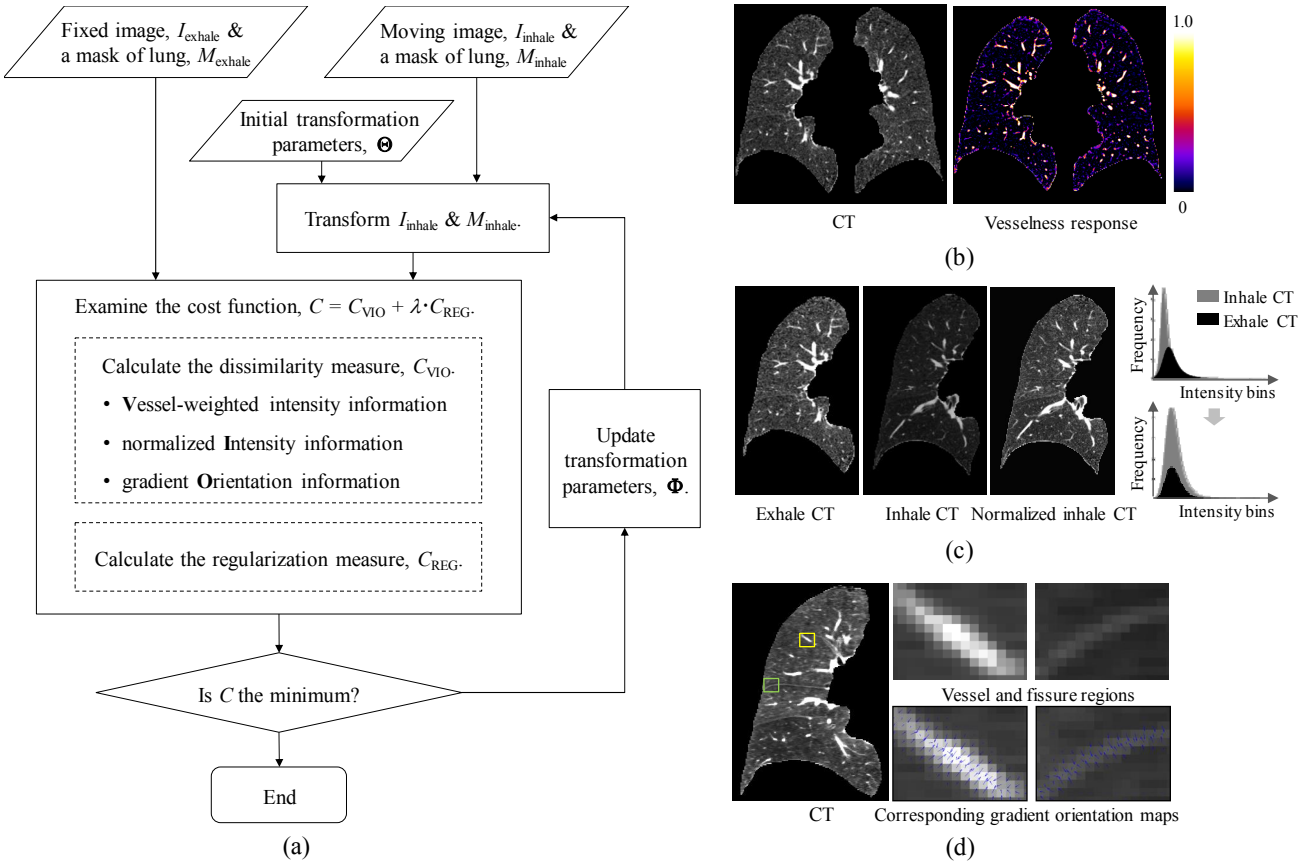

Figure 1. (a) Block diagram of the proposed non-rigid registration framework and three components consisting of the proposed dissimilarity measure, namely (b) vessel-weighted intensity information, (c) normalized intensity information, and (d) gradient orientation information.

2.1 Transformation

To compensate for the local deformation between the two images due to respiration, we adopt the B-spline free form deformation (FFD) model as a transformation kernel [17]. The FFD model is defined by the displacement coefficients of

a set of sparse and uniformly-spaced control points, which are denoted as $\mathbf{\Phi}$. Here, the control points act as transformation parameters of the B-spline FFD, which should be found through computation.

2.2 Cost function based on the proposed dissimilarity measure

Since pulmonary vessels are widely distributed and well defined in both lung CT images, they help to guide the registration process converged well by providing the strong feature information even in a large motion environment. Hence, we first associate the vessel-weighted intensity information (see figure 2(b).) with the dissimilarity measure obtained by using the multi-scale vesselness response metric [18]. To improve the registration accuracy in the other structural regions such as bronchi, fissures, emphysematous cysts, and especially lung boundaries distant from vessels, we also take the intensity information into the dissimilarity measure. The large volume deformations due to respiration lead to significant intensity change in the CT image. To produce better intensity correlation between the exhale and inhale CT images, we utilize it after intensity normalization via histogram matching [19] that modifies the histogram of inhale CT image, thereby being similar to that of exhale CT image (see figure 2(c).). Meanwhile, the registration accuracy may be limited in the parenchymal regions and the structural regions with low intensity contrast. That is because they have little information enough to guide to find the reliable transformation and give almost no contribution to the registration process. To alleviate this problem and improve the accuracy for all lung regions, we suggest to consider the gradient orientation information (see figure 2(d).), which can associate the spatial information, in the dissimilarity measure.

Based on the three components described above, we define the dissimilarity measure C_{VIO} as

$$C_{\mathrm{VIO}} = \lambda_1 \cdot C_{\mathrm{SSVRD}} + \lambda_2 \cdot C_{\mathrm{SSNID}} + \lambda_3 \cdot C_{\mathrm{NGF}}, \tag{1}$$

where

$$C_{\mathrm{SSVRD}} = \frac{1}{N_\Omega} \sum_{\mathbf{x} \in \Omega} [V_{\mathrm{exhale}}(\mathbf{x}) - V_{\mathrm{inhale}}(\mathbf{r}(\mathbf{x}; \mathbf{\Theta}, \mathbf{\Phi}))]^2, \tag{2}$$

$$C_{\mathrm{SSNID}} = \frac{1}{N_\Omega} \sum_{\mathbf{x} \in \Omega} [N_{\mathrm{exhale}}(\mathbf{x}) - N_{\mathrm{inhale}}(\mathbf{r}(\mathbf{x}; \mathbf{\Theta}, \mathbf{\Phi}))]^2, \text{ and} \tag{3}$$

$$C_{\mathrm{NGF}} = \frac{1}{N_\Omega} \sum_{\mathbf{x} \in \Omega} 1 - [\widetilde{\nabla} I_{\mathrm{exhale}}(\mathbf{x})^T \cdot \widetilde{\nabla} I_{\mathrm{inhale}}(\mathbf{r}(\mathbf{x}; \mathbf{\Theta}, \mathbf{\Phi}))]^2. \tag{4}$$

Here, λ_1, λ_2, and λ_3 are the weighting parameters for each cost component. $\mathbf{x}$ is a voxel point in the masked region of the exhale CT image, Ω, and $\mathbf{r}(\mathbf{x}; \mathbf{\Theta}, \mathbf{\Phi})$ is the transformation which gives the corresponding location in the inhale CT image to $\mathbf{x}$. $V(\cdot)$ and $N(\cdot)$ are the vesselness response and the normalized intensity images for a given CT image which are rescaled to [0, 1], respectively. $\widetilde{\nabla} I(\cdot)$ denotes the normalized gradient field (NGF) [20] of a CT image, which is determined as, $\widetilde{\nabla} I(\mathbf{x}) = \nabla I(\mathbf{x}) / \sqrt{\| \nabla I(\mathbf{x}) \|^2 + \eta^2}$ where η is an edge parameter that controls the influence of small edges due to noise.

In order to constrain the transformation to be smooth and prevent abrupt changes in the displacement fields, we adopt the curvature model based regularization cost, C_{REG}, which is represented as

$$C_{\mathrm{REG}} = \frac{1}{N_\Omega} \sum_{\mathbf{x} \in \Omega} \left\| \nabla^2 (\mathbf{r}(\mathbf{x}; \mathbf{\Theta}, \mathbf{\Phi}) - \mathbf{x}) \right\|^2. \tag{5}$$

Using the dissimilarity measure, C_{VIO} and the regularization measure, C_{REG} described above, we finally define the cost function, C as

$$C = C_{\mathrm{VIO}} + \lambda_{\mathrm{REG}} \cdot C_{\mathrm{REG}}, \tag{6}$$

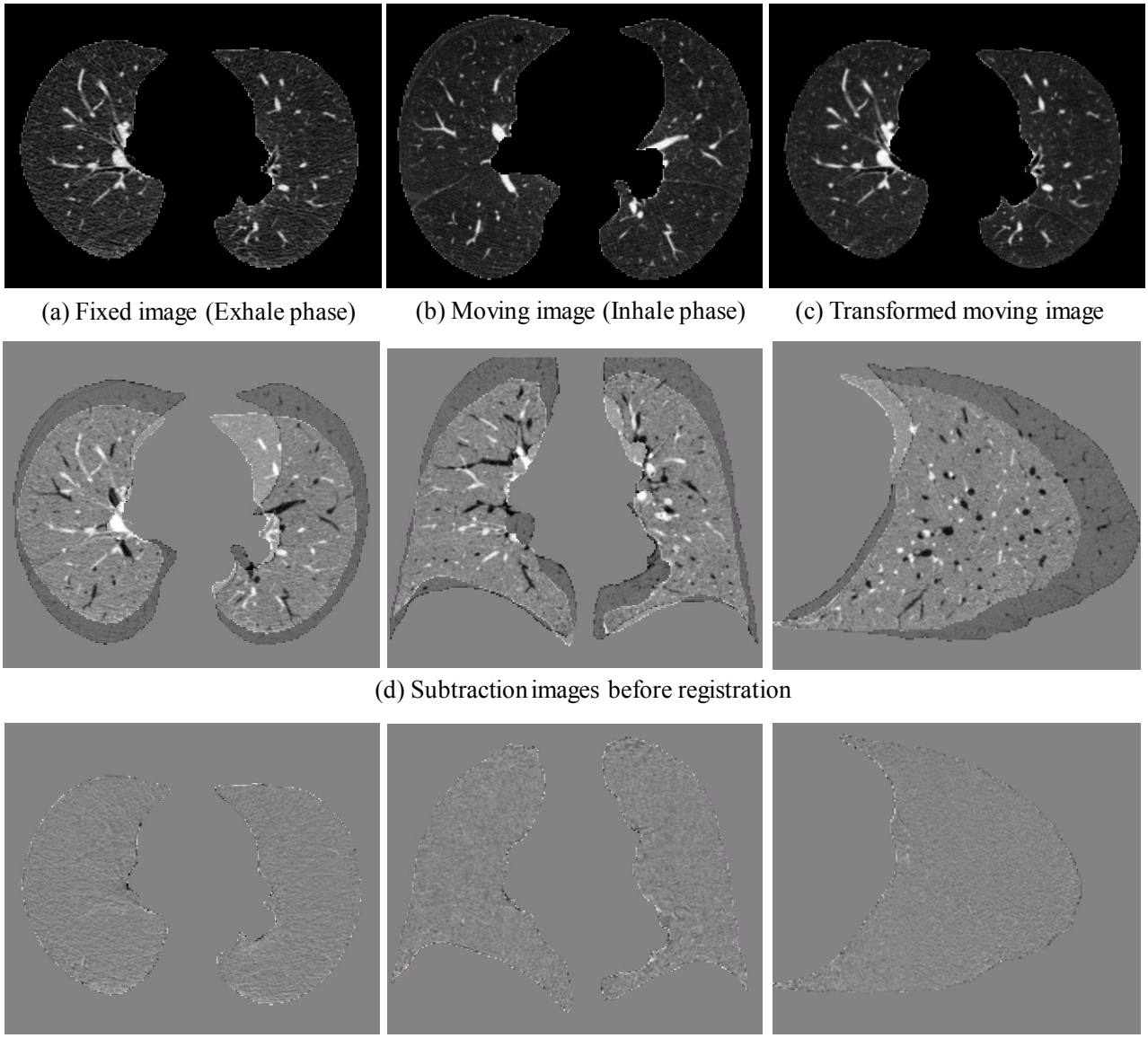

Figure 2. Result of the proposed registration method for clinical dataset #4. Top row, left to right: Axial slice in fixed (exhale), moving (inhale) and transformed moving image. Middle row, left to right: Subtraction images before registration in axial, coronal and sagittal view. Bottom row, left to right: Subtraction images after registration.

where λ_{REG} is the weighting parameters which represents the tradeoff between the alignment accuracy of two images, C_{VIO} and the smoothness of transformation, C_{REG}.

2.3 Optimization

To determine the optimal set of transformation parameters, $\mathbf{\Phi}$, we minimize the cost function of eq. (6) by using the non-linear conjugate gradient decent algorithm [21]. Here, in order to improve the computational efficiency while avoiding local minima, we adopt a multi-resolution scheme [17] which utilizes a coarse to fine optimization.

3. EXPERIMENTAL RESULTS

To evaluate the performance of the proposed non-rigid registration algorithm, we use six clinical lung CT datasets. In each clinical case, two different respiratory 3D CT images were acquired with a breath-hold at the exhale and inhale phases, respectively. The typical image dimensions and voxel size were 512 x 512 x 380 and 0.75 x 0.75 x 0.7mm^3, respectively. The weighting parameters, λ_1, λ_2, λ_3, and λ_{REG} were empirically set to 0.4, 0.4, 0.2, and 0.02, respectively, and the edge parameter, η was set to 50.

Figure 2 shows the result of the proposed registration method for clinical dataset #4. Based on the subtraction images before and after registration, it is confirmed that the large displacement between the two images due to respiration was successfully corrected. In order to evaluate the performance quantitatively, we utilized two representative criteria: average landmark distances (with a unit of *mm*) on more than 100 distributed landmark pairs mostly selected at airway or vessel branch points, and lung volume overlap ratio based on dice similarity criterion (with a unit of percentage). In the table 1, it is shown that the proposed dissimilarity measure, C_{VIO} delivered the most precise registration accuracy compared to those of other competitive methods in terms of both criteria.

To cope with the memory and/or execution time limitations, a half-resolution image pair may be preferred to a full-resolution image pair. To minimize the performance decrease due to information loss by the resolution degradation, we suggest to apply the multi-resolution scheme that is combined with the variable grid size as described in the table 2(b), rather than that combined with the constant grid size as in the table 2(a). As shown in the table 2(c) and figure 3, in spite of using the half-resolution image pair, the suggested multi-resolution scheme yielded the almost comparable registration accuracy to that of existing multi-resolution scheme based on a full-resolution image pair.

Table 1. Comparisons of landmark distances in *mm* and lung volume overlap ratio before and after registration. (*SSVRD: sum of squired vesselness response difference, **SSNID: sum of squired normalized intensity difference).

Datasets	Before registration	After registration				
		SSID	SSVRD*	NGF	SSNID** + SSVRD	Proposed
Set 1	15.803 (82.1%)	0.751(98.6%)	0.718 (98.1%)	0.720 (98.1%)	0.722 (98.8%)	0.710 (98.9%)
Set 2	24.474 (65.0%)	1.521 (98.3%)	0.775 (95.5%)	0.866 (97.1%)	0.749 (98.8%)	0.747 (98.8%)
Set 3	20.722 (82.6%)	1.595 (95.7%)	0.762 (97.3%)	0.750 (98.3%)	0.987 (98.7%)	0.748 (99.0%)
Set 4	32.870 (68.1%)	1.371 (91.6%)	0.835 (93.9%)	0.795 (97.4%)	0.816 (98.6%)	0.781 (98.4%)
Set 5	30.669 (70.0%)	1.215 (90.7%)	0.957 (95.4%)	1.020 (96.5%)	0.944 (98.3%)	0.914 (98.5%)
Set 6	35.740 (66.4%)	1.436 (92.8%)	0.852 (94.6%)	1.066 (95.6%)	0.910 (96.2%)	0.817 (98.3%)
Average	**26.713 (72.4%)**	**1.315 (94.6%)**	**0.817 (95.8%)**	**0.869 (97.1%)**	**0.855 (98.2%)**	**0.787 (98.6%)**

Table 2. Multi-resolution schemes based on (a) a constant-grid size and a full-resolution image, and (b) a variable-grid size and a half-resolution image, and (c) comparisons of landmark distances in *mm* after registration based on the proposed dissimilarity measure, depending on different multi-resolution schemes.

Resolution level	Image size (voxels)	Control point grid size (voxels)	Transformation model size
Level 1	128x128x128	10	16x16x16
Level 2	256x256x256	10	29x29x29
Level 3	512x512x512	10	55x55x55

(a)

Resolution level	Image size (voxels)	Control point grid size (voxels)	Transformation model size
Level 1	128x128x128	16	11x11x11
		8	19x19x19
Level 2	256x256x256	8	35x35x35
		4	67x67x67
		2	131x131x131

(b)

3-level multi-resolution optimization based on a full-resolution image	2-level multi-resolution optimization based on a half-resolution image	
With a constant grid size	**With a constant grid size**	**With a variable grid size**
0.787	1.000	0.797

(c)

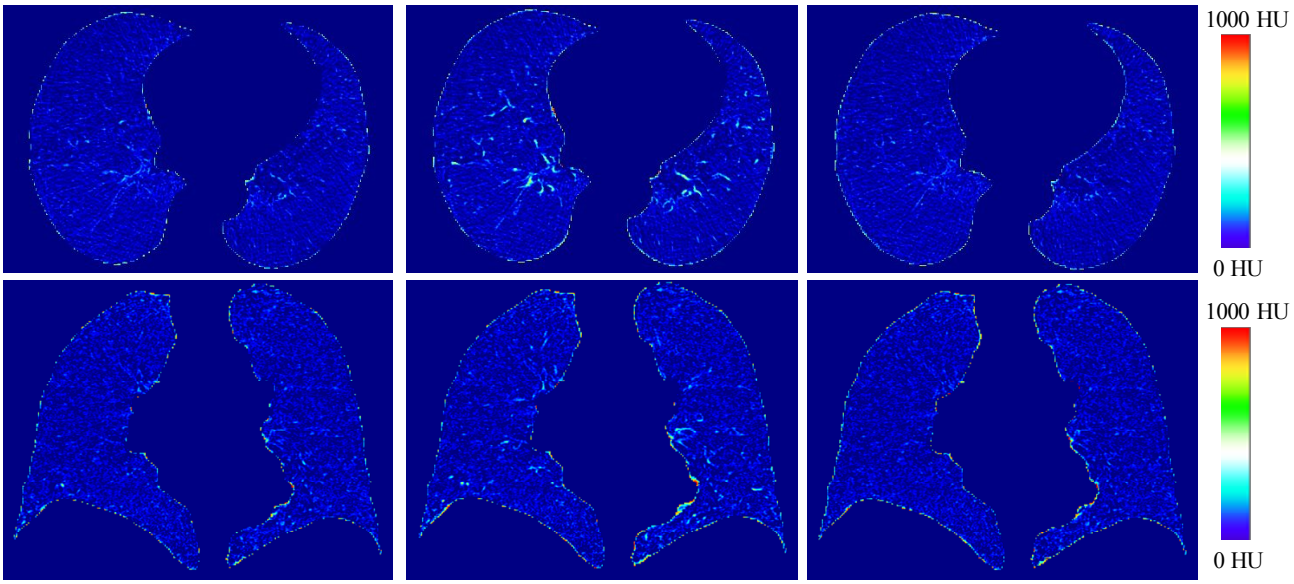

Figure 3. Comparison of registration results depending on different multi-resolution schemes for clinical dataset 1. Difference images after registration using (a) 3-level multi-resolution scheme based on a constant-grid-size and a full-resolution image, (b) 2-level multi-resolution scheme based on a constant-grid-size and a half-resolution image, and (c) 2-level multi-resolution scheme based on a variable-grid-sizes and a half-resolution image.

4. CONCLUSIONS

In this paper, we present a non-rigid registration algorithm between exhale and inhale CT images of the lung. For registration, we introduce the new dissimilarity measure, which uses vessel-weighted intensity, normalized intensity information, and gradient orientation information. Since the measure effectively exploits spatial correlation as well as intensity correlation, we can enhance the non-rigid registration accuracy even in the large displacement environment due to respiration and ambiguous intensity mapping relations between two images. We also investigate the meaningful multi-resolution scheme using variable grid sizes, which can alleviate the accuracy degradation in case that a half-resolution image pair has to be adopted due to memory and/or execution time limitations.

REFERENCES

[1] Keall P. J., Siebers J. V., Joshi S., and Mohan R., "Monte Carlo as a four-dimensional radiotherapy treatment-planning tool to account for respiratory motion," Phys. Med. Biol. 49, 3639-3648 (2004).

[2] Rietzel E., Chen G. T., Choi N. C., and Willet C. G., "Four-dimensional image-based treatment planning: Target volume segmentation and dose calculation in the presence of respiratory motion," Int. J. Radiat. Oncol. Biol. Phys. 61, 1535-1550 (2005).

[3] Sarrut D., Delhay B., Villard P. F., Boldea V., Beuve M., and Clarysse P., "A comparison framework for breathing motion estimation methods from 4-D imaging," IEEE Trans. Med. Imaging 26, 1636-1648 (2007).

[4] Haider C. R., Bartholmai B. J., Holmes D. R., Camp J. J., and Robb R. A., "Quantitative characterization of lung disease," Comput. Med. Imaging Graph. 29, 555-563 (2005).

[5] Torigian D. A., Gefter W. B., Affuso J. D., Emami K., and Dougherty L., "Application of an optical flow method to inspiratory and expiratory lung MDCT to assess regional air trapping: A feasibility study," Am. J. Roentgenol. 188, 276-280 (2007).
[6] Low D. A., Parikh P. J., Lu W., Dempsey J. F., Wahab S. H., Hubenschmidt J. P., Nystrom M. M., Handoko M., and Bradley J. D., "Novel breathing motion model for radiotherapy," Int. J. Radiat. Oncol. Biol. Phys. 63, 921-929 (2005).
[7] Ue H., Haneishi H., Iwanaga H., and Suga K., "Respiratory lung motion analysis using a nonlinear motion correction technique for respiratory-gated lung perfusion SPECT images," Ann. Nucl. Med. 21, 175-183 (2007).
[8] Christensen G. E., Song J. H., Lu W., Naqa I. E., and Low D. A., "Tracking lung tissue motion and expansion/compression with inverse consistent image registration and spirometry," Med Phys. 34(6), 2155-2163 (2007).
[9] Sarrut D., Boldea V., Miguet S., and Ginestet C., "Simulation of four-dimensional CT images from deformable registration between inhale and exhale breath-hold CT scans, " Med Phys. 33(3), 605–617 (2006).
[10] Sundaram T. A. and Gee J. C., "Towards a model of lung biomechanics: pulmonary kinematics via registration of serial lung images," Medical Image Analysis 9(6), 524-537 (2005).
[11] Mattes D., Haynor D. R., Vesselle H., Lewellen T. K., and Eubank W., "PET-CT image registration in the chest using free-form deformations," IEEE Trans. Med. Imaging 22(1), 120-128 (2003).
[12] Gorbunova V., Lo P., Ashraf H., Dirksen A., Nielsen M., and de Bruijne M., "Weight preserving image registration for monitoring disease progression in lung CT," Proceedings of MICCAI, 863-870 (2008).
[13] Yin Y., Hoffman E. A., and Lin C. L., "Mass preserving nonrigid registration of CT lung images using cubic B-spline," Med Phys. 36(9), 4213-4222 (2009).
[14] Cao K., Ding K., Reinhardt J. M., and Christensen G. E., "Improving Intensity-Based Lung CT Registration Accuracy Utilizing Vascular Information," Int J Biomed Imaging 2012(3), 1-17 (2012).
[15] van Rikxoort E. M., de Hoop B., Viergever M. A., Prokop M., and van Ginneken B., "Automatic lung segmentation from thoracic computed tomography scans using a hybrid approach with error detection," Med Phys. 36, 2934-2947 (2009).
[16] Press W. H., Teukolsky S. A., Vetterling W. T., and Flannery B. P., "Downhill simplex method in multidimensions," Numerical Recipes: The Art of Scientific Computing, 289-293 (1986).
[17] Rueckert D, Sonoda L. I. , Hayes C., Hill D. L. G., Leach M. O., and Hawkes D. J., "Nonrigid registration using free-form deformations: application to breast MR images," IEEE Trans. Med. Imaging 18, 712-721 (1999).
[18] Frangi A. F., Niessen W. J., Vincken K. L., and Viergever M. A., "Multiscale vessel enhancement filtering," Medical Image Computing and Computer-Assisted Intervention, 130-137 (1998).
[19] Shen D., "Image registration by local histogram matching," Pattern Recognition 40, 1161-1172 (2012).
[20] Hodneland E., Lundervold A., Rørvik J., and Munthe-Kaas A. J., "Normalized gradient fields for nonlinear motion correction of DCE-MRI time series," Computerized Medical Imaging and Graphics 38, 202-210 (2014).
[21] Klein S., Staring M., and Pluim J. P., "Evaluation of optimization methods for nonrigid medical image registration using mutual information and B-splines," IEEE Trans. Med. Imaging 16, 2879-2890 (2007).